ROYAL SOCIETY OF CHEMISTRY

PAPER

Tailoring carbon-encapsulated gold nanoclusters *via* microchip laser ablation in polystyrene solution: controlling size, structure, and photoluminescent properties†

Barana Sandakelum Hettiarachchi, [iD] [a]
Yumi Yakiyama [iD] *[abc] and Hidehiro Sakurai [iD] *[ab]

The desired control of size, structure, and optical properties of laser-derived carbon-encapsulated metal nanoclusters (NCs) is crucial for various applications. This study introduces a novel approach utilizing a microchip laser (MCL) ablation for preparing carbon-encapsulated gold nanoclusters (Au NCs) in a toluene solution, employing polystyrene as a stabilizing agent. Through systematic experiments, control over NC size and carbon layer thickness is achieved by adjusting laser power and polystyrene concentration. Lower laser power combined with higher polystyrene concentration yields smaller Au NCs with thinner carbon layers, demonstrating the efficacy of this approach. Additionally, the prepared nanostructures exhibit enhanced photoluminescence properties, with emissions dependent on excitation wavelength and carbon layer thickness. These findings underscore the potential of MCL-based pulsed laser ablation in liquid in deriving carbon-encapsulated metal NCs, highlighting the importance of experimental parameters and solvent characteristics in tailoring NC properties.

Introduction

Carbon-encapsulated metal nanoparticles (NPs) have emerged as a promising field of study owing to their various applications ranging from catalysis to biomedical engineering.[1,2] These nanostructures possess unique characteristics, particularly their exceptional catalytic performance in Fenton-like systems.[3] In addition, heteroatom dopants, such as metal NPs encapsulated in N, P-doped carbon,[4] and the favourable interface between metal and carbon, have been observed to facilitate efficient electron transfer, enhancing catalytic activity.[5] The preparation of carbon-encapsulated metal NPs typically involves the reduction of metal ions, followed by encapsulation within a carbon shell.[6] Various methods exist for coating the NP surface, including vapor deposition,[7] sol–gel,[8] and solution dipping.[9] Pulsed laser ablation in liquid (PLAL) is

a promising technique for fabricating such nanostructured materials in a single step, offering ease and effectiveness in ambient conditions.[10–12]

In the PLAL process, metal NPs are generated within a plasma plume by subjecting a metal target to intense laser pulses. Under the high-temperature and high-pressure conditions of the plasma plume, solvent molecules decompose, forming carbon species. These carbon species then condense onto the surface of the metal particles, resulting in an encapsulated nanostructure.[10,13–15] Among the commonly used solvents for PLAL, toluene or benzene are used as solvents and carbon sources to prepare carbon-encapsulated metal NPs. It is known that the thickness of the outer carbon layer plays a crucial role in the performance of carbon-encapsulated metal NPs, particularly in applications such as surface-enhanced Raman scattering (SERS),[16] where ultrathin layers are desirable for maximizing SERS efficiency and desirable for controlling the surface plasmon properties of Au NPs. Additionally, reducing particle size enhances the number of surface sites per unit area of metals, leading to superior catalytic properties.[17] However, achieving smaller-sized NPs with ultrathin carbon layers remains a challenge.

In our recent studies, we demonstrated the ability of MCL to produce Au NPs in both aqueous and polar organic medias (Fig. S1†).[18,19] Especially in the latter case, we explored the formation of Au nanoclusters (NCs), having below 2 nm

[a] Division of Applied Chemistry, Graduate School of Engineering, Osaka University, 2-1 Yamadaoka, Suita, Osaka 565-0871, Japan.
E-mail: yakiyama@chem.eng.osaka-u.ac.jp, hsakurai@chem.eng.osaka-u.ac.jp
[b] Innovative Catalysis Science Division, Institute for Open and Transdisciplinary Research Initiatives (ICS-OTRI), Osaka University, 2-1 Yamadaoka, Suita, Osaka 565-0871, Japan
[c] PRESTO, Japan Science and Technology Agency (JST), Kawaguchi, Saitama 332-0012, Japan

† Electronic supplementary information (ESI) available: Supporting figures, tables, and Mie theory calculations. See DOI: https://doi.org/10.1039/d4lf00349g

diameter, stabilized by poly(N-vinyl-2-pyrrolidone) (PVP), a hydrophilic polymer. Indeed, the use of MCL addresses the limitations of high-power laser systems when working with flammable organic solvents, making it a promising technique for advanced NP synthesis. Motivated by such attractive features of MCL system, here we extended our research by using polystyrene as a hydrophobic polymer in toluene. The use of polystyrene in this experiment realized the control of particle size distribution and toluene decomposition due to its high heat capacity,[20] resulting the mono-dispersed small Au NC with thin carbon layer. Furthermore, we observed that the laser ablation-derived carbon layer exhibits emission in the visible spectral region with wavelength-dependent properties similar to typical carbon dots, adding to these novel nanomaterials' versatility and potential applications.

Results and discussion

Au NCs preparation by PLAL

Our experiment was initiated with 180 mW laser irradiation on a bulk gold target in a 50 mM polystyrene-dissolved toluene solution for an hour. During the ablation process, the colour of the solution turned from colourless to brown. As shown in Fig. 1(a–c), TEM analysis confirmed the formation of Au NCs with a primary particle size of 1.7 ± 0.3 nm and a very narrow particle size distribution. This observed primary particle size aligns with the literature, in which carbon materials are produced by PLAL using toluene.[10,14] In general, PLAL affords metal NPs with more than 5 nm.[21] The observed characteristics of the particles in this experiment suggested that the encapsulation of Au particles within a carbon matrix generated by solvent decomposition plays a significant role in the process. This encapsulation effectively inhibits particle nucleation and growth, resulting in smaller primary particle sizes. Simultaneously, we prepared Au NC in toluene solvent without using polystyrene. As shown in Fig. 1(d–f), obtained

Au NCs showed three different primary particle size fractions (1.8 nm 19%, 2.8 nm 44%, 4.5 nm 37%) covered by thicker graphitic carbon layers. This result differs from previous literature affording mono size distribution,[10] probably due to the larger laser fluence of the current system (19.6 J cm^{-2}). Considering previous reports about the NP formation,[15,22] the plausible mechanisms for the formation of different sizes of carbon encapsulated nanostructures is proposed as shown in Fig. 2. When a pulsed laser irradiates the bulk gold target, Au particles are ablated under the high-temperature and high-pressure of the plasma plume. As recent studies have demonstrated and that particle growth begins within the plasma plume during the first nanoseconds of the process, then eventually produces several size distributions.[23,24] Under these extreme conditions, toluene molecules immediately decompose, generating carbon species. These carbon species subsequently condense onto the ablated Au particles, forming the carbon layer. In the absence of a stabilizing agent, the resulting nanostructures undergo several aggregation stages due to Brownian motion and van der Waals forces.[25] In contrast, under the presence of polystyrene, the adsorption of polystyrene onto the surface of the forming Au core and/or the carbon layer covering the Au core inhibits further growth of Au core and aggregation of the resulting nanostructures. This leads to small and uniform sized particles. When we next focus on the carbon layer thickness (Fig. 1(b) and S2†), it was found that the condition with polystyrene gave relatively thinner layer. It is reasonably suggested that the size of NCs affects the carbon layer thickness in terms of the cooling effect (pyrolysis of carbon)[22] and decomposed carbon distribution around the plume (segregation of carbon).[26] Indeed, the slightly larger cluster size of the samples obtained under the absence of polystyrene indicate the contribution of the above two effects. Additionally, the high heat capacity of polystyrene reduces the extent of toluene decomposition, resulting in thinner carbon layers.

In addition to analysing the primary particle size, we evaluated the secondary particle size using dynamic light scattering (DLS), which highlights the structural differences in PLAL products formed with and without polystyrene. As modelled in Fig. 3, the sample containing polystyrene exhibits an average secondary particle diameter of 7.3 nm. In contrast, the pure toluene sample has a significantly larger average diameter of 2.4 × 10^2 nm, corresponding to the aggregated carbon structures as confirmed in TEM analysis.

Raman spectral measurements showed the detailed aspects of the carbon layer (Fig. S3†). Each sample showed two broad peaks: around 1350 cm^{-1} and 1570 cm^{-1}, corresponding to the D and G bands of carbon, respectively. The carbon structure in our samples was very similar to those obtained by Chieu *et al.* from the pyrolysis of benzene, as evidenced by the similarity in the Raman spectra.[27]

The UV/visible absorption spectra revealed that both prepared samples exhibit similar absorption characteristics (Fig. S4†). A broad surface plasmon resonance (SPR) peak
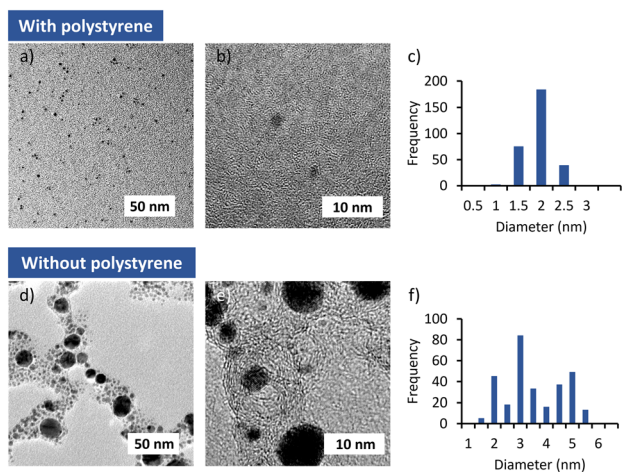

Fig. 1 a), b), d) and e) TEM images and c) and f) size distribution of Au NCs prepared a)–c) under polystyrene and d)–f) in the absence of polystyrene. The applied average energy was 180 mW for each.
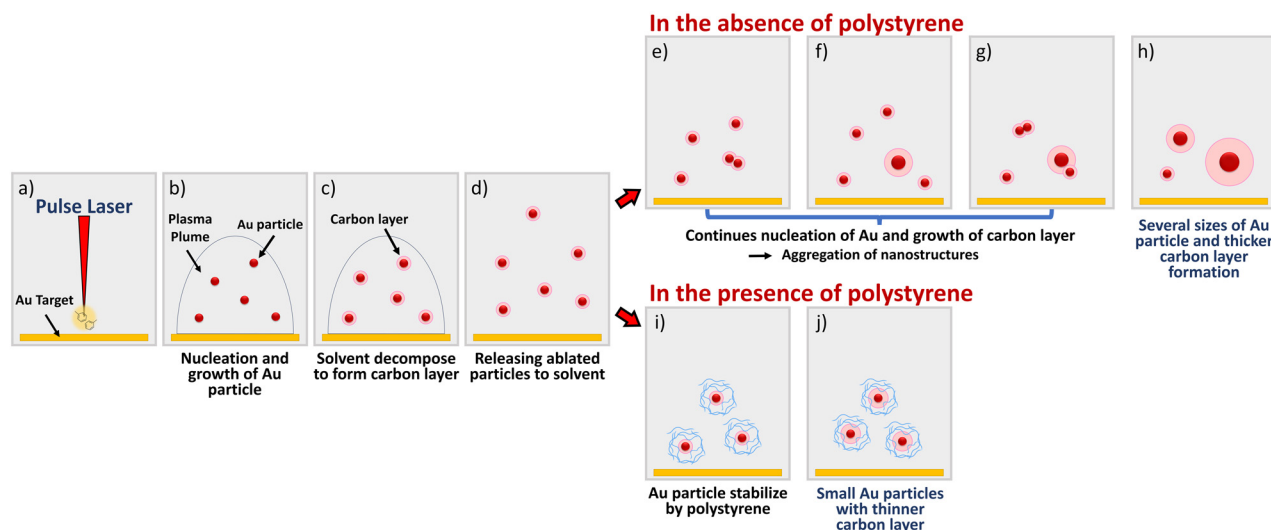
© 2025 The Author(s). Published by the Royal Society of Chemistry

RSC Appl. Interfaces, 2025, **2**, 772–779 | 773

Fig. 2 Schematic representation of the formation of carbon-encapsulated nanostructures. When a pulsed laser irradiates a bulk gold target (a), Au particles are ablated in the plasma plume (b). The decomposition of toluene generates carbon, which condenses onto the surface of the Au particles, forming carbon-encapsulated nanostructures (c). Then, these nanostructures are released to the surrounding solvent (d). In the absence of a stabilizing agent, these nanostructures tend to aggregate, leading to growth in particle size and an increase in the number of carbon layers (e)–(g). Thus, nanostructures with varying sizes are produced (h). In the presence of polystyrene, which adsorbs polystyrene onto the encapsulated nanostructures, further aggregation is prevented (i) and (j).

was observed, which was more prominent in the sample prepared without polystyrene. It is known that the SPR peak shape is affected by several factors, such as of course the presence of outer layer, which allows the delocalization of free electrons at the interface region,[28] and the electron–phonon and phonon–phonon relaxation, which are enhanced especially in the case with <20 nm sized NPs to give broader peak.[29] These factors seemed to contribute to the overall suppression and broadening of the SPR peak in our samples.

Based on the analysis of TEM and UV/visible absorption spectra, it is evident that the carbon matrix not only regulates the growth of NCs but also diminishes the SPR of the generated Au NCs. Thus, the carbon-encapsulated Au NCs possess zero plasmonic properties, with their primary role being to support carbon formation. However, it is crucial to obtain carbon-encapsulated Au NCs with plasmonic properties, as it enhances their tunability and functionality of the NCs for various applications ranging from sensing and catalysis to biomedical uses. In the context of PLAL, several authors have attempted to achieve plasmonic properties

using different approaches. For instance, in ref. 10, the authors successfully recovered the Au NCs SPR by oxidizing the carbon layer. However, Au NC aggregation occurred, and they could not maintain the constant particle size even after oxidizing the carbon layer. In contrast, ref. 13 reported obtaining ultrathin carbon layers, controlled from 0.6 to 2 nm, wrapped around Au particles through laser ablation in ethanol/toluene mixed solution. However, the inner noble metal size was reported to be <20 nm. Notably, neither publication provided information on the most effective method for producing very small metal NCs with ultrathin carbon layers. Thus, our experiment aimed to effectively control both the size of Au NCs and the thickness of the carbon layer by following two approaches: changing the laser power and changing the heat capacity of toluene.

Laser power effect on carbon-encapsulated Au NC size

The control of heat energy in the laser-ablated plasma plume is crucial because it directly influences the energy transfer required for the decomposition of toluene. In other words, we can change the carbon layer thickness by adjusting the
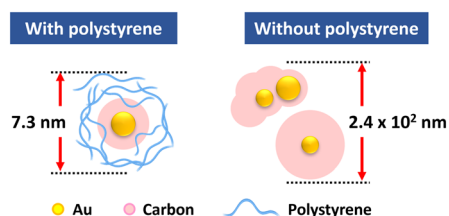

Fig. 3 Schematic structural model and secondary particle size of carbon-encapsulated Au NCs in the presence and absence of polystyrene (after 15 minutes of sonication).

Table 1 Primary particle diameter (determined *via* TEM analysis) of Au NCs prepared by PLAL under the presence of polystyrene (50 mM) with different laser powers. See (ESI†) for TEM images of each sample

Laser power (mW)	Primary particle size (nm)	Carbon layer thickness (nm)
104	2.2 ± 0.4	2.4 ± 0.2
180	1.7 ± 0.2	3.0 ± 0.3
350	1.8 ± 0.4	3.5 ± 0.2
550	1.7 ± 0.3	4.2 ± 0.3

laser power. In this context, the ablation experiments were performed in four different laser powers (104, 180, 350, 550 mW) by modifying the pulse current (Table 1). As shown in Fig. 1, the use of polystyrene is important for achieving smaller particle sizes, improving dispersion, and preventing aggregation. Therefore, the laser power was varied while maintaining a 50 mM concentration of polystyrene. Here, carbon layer thickness was evaluated using an extension of Mie theory designed for core–shell structures, where carbon is considered the outer shell and Au NCs are the core, as described in previous studies (see ESI†).[10] It can be seen from the TEM particle size (Fig. S5†) and carbon layer thickness results (Table 1) that the thickness of the carbon layer surrounding the inner Au NCs is greatly influenced by laser irradiation power. A thin carbon layer is achieved by decreasing the laser power, resulting in smaller amount of solvent decomposition. It is noteworthy that under very low power conditions, particularly at 104 mW, Au NCs' size was slightly larger. Because, at lower laser power, the heat from the laser-generating plasma plume may not be sufficient to induce significant decomposition of toluene molecules. This results in slower carbon layer formation, allowing more time for the Au NCs to aggregate and grow, forming a larger size. Thus, 104 mW laser power is suitable for forming an ultrathin carbon layer, although controlling the Au NC size under this condition is difficult. Conversely, under very high laser power, the thick carbon layer fully controls the size of Au NCs. Fig. 4(a) shows the UV-vis spectra of carbon-encapsulated Au NCs prepared under varying laser powers. The data reveals that the quenching effect of SPR diminishes as the thickness of the carbon layer decreases at low laser power, which results in the generation of the plasmon properties. This significant red shift in the SPR peak of Au NCs occurs compared to the typical peak at around 520 nm due to the high refractive index (n) of the carbon layer ($n = 2.7$)[30] compared to toluene ($n = 1.5$), which serves as the surrounding medium of Au NCs.[31]

medium. Toluene has a relatively low heat capacity, causing it to decompose quickly when exposed to the heat energy under the high-temperature and high-pressure of the plasma plume. In contrast, polystyrene typically possesses higher heat capacities due to its molecular structure and larger molecular weight. Using differential scanning calorimetry analysis, we experimentally measured the heat capacity of toluene (1.1 ± 0.1 J K^{-1}), 200 mM polystyrene in toluene (4.6 ± 0.1 J K^{-1}), and 400 mM polystyrene in toluene (6.1 ± 0.2 J K^{-1}). These results indicate that increment of the polystyrene content gains the heat capacity of the system, reducing toluene decomposition and the carbon layer thickness. In addition, presence of polystyrene contributed the formation of smaller Au particles. Laser ablation experiments with different polystyrene concentration will tell the further detail of the effect of polystyrene. In this context, six different polystyrene concentrations (0, 10, 50, 100, 200, and 400 mM) were investigated, while maintaining constant laser power at 104 mW as previously applied (Fig. S6†). The results presented in Table 2 clearly show that the polystyrene concentration strongly influences the primary particle size of the Au NCs and thickness of the outer carbon layer. It is evident that increasing the polystyrene concentration the size of the Au NCs becomes smaller due to polystyrene acting as a stabilizing agent and preventing aggregation. In addition, as the polystyrene concentration increases, leads to a decrease in the solvent decomposition, resulting in a thinner carbon layer. This outcome further demonstrates that even under laser irradiation with low power, smaller Au NC sizes can be achieved by increasing the polystyrene concentration. Thus, low power with high polystyrene concentration is more effective in obtaining a small core with a thin carbon layer. The UV-vis spectra of Au NCs prepared with different concentrations of polystyrene are presented in Fig. 4(b). This demonstrates that the reduction in the SPR quenching effect is noticeable when a thin carbon layer is present. Consequently, this process leads to the formation of carbon-encapsulated Au NCs with plasmonic properties.

Polystyrene concentration effect on carbon-encapsulated Au NC size

Our second approach involves controlling solvent decomposition by increasing the polystyrene content in the laser ablation

Perspectives of MCL ablation

A PLAL experiment was conducted using both the MCL and a higher-power ns-laser (Quanta-Ray PRO-250) under optimized polystyrene concentration (400 mM) to evaluate the effectiveness of the MCL in obtaining a thinner carbon layer,
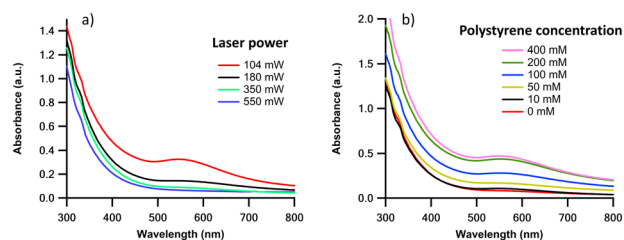

Fig. 4 The UV-vis spectrum of carbon-encapsulated Au NCs obtained by using a) different laser powers in 50 mM polystyrene/toluene solution and b) different polystyrene concentrations with applying 104 mW average power. All the samples were prepared as 0.03 mM Au in THF.

Table 2 Results of PLAL on gold target in toluene under different concentrations of polystyrene. The average laser power was fixed to be 104 mW

Polystyrene concentration (mM)	Particle size (nm)	Carbon layer thickness (nm)
0	2.8 ± 0.5	3.9 ± 0.6
10	2.5 ± 0.5	3.3 ± 0.6
50	2.2 ± 0.3	2.4 ± 0.4
100	1.7 ± 0.3	2.1 ± 0.4
200	1.7 ± 0.2	2.0 ± 0.4
400	1.7 ± 0.2	1.8 ± 0.4

© 2025 The Author(s). Published by the Royal Society of Chemistry

RSC Appl. Interfaces, 2025, **2**, 772–779 | 775

Table 3 Results and PLAL parameters of the present MCL system and the ns-laser (Quanta-Ray PRO-250) system in a comparison experiment

	Present MCL	Quanta-Ray PRO-250
Pulse energy (mJ)	1.3	25
Pulse duration (ns)	0.9	12
Spot diameter (μm)	130 ± 6	800 ± 13
Laser fluence (J cm^{-2})	19.6	9.95
Repetition rate (Hz)	100	10
Particle size (nm)	1.7 ± 0.3	1.7 ± 0.3
SPR band	Present	Absent

following the laser conditions outlined in Table 3. The results demonstrated that the SPR band is strongly suppressed for the Au NCs produced by the higher-power laser. Meanwhile the Au NCs produced by the MCL system show a distinct SPR band, as shown in Fig. 5. This suppression is probably attributable to the forming of a thicker carbon layer resulting from the higher pulse energy of the Quanta-Ray PRO-250 derived from the longer pulse duration. This result clearly reflected the MCL's feature of high-power laser showed a comparable particle size of 1.7 ± 0.3 nm to the case of MCL with a narrow particle size distribution (Fig. S7†), reflecting a half laser fluence of Quanta-Ray machine compared with MCL's, which does not cause significant difference in the particle size in the reported work.[32]

Photoluminescence properties of carbon-encapsulated Au NCs

Carbon nanomaterials are emerging as promising photoluminescence (PL) materials, gaining significant interest due to their potential applications.[33,34] This motivated us to investigate the PL properties of MCL-generated carbon in encapsulated nanostructures. Understanding the optical behavior, specifically how the emission spectra change with parameters such as excitation wavelength and carbon layer thickness, is important. Thus, our study first focused on the excitation wavelength dependency of carbon-encapsulated Au NCs having the smallest Au cores and thinnest carbon layers. This
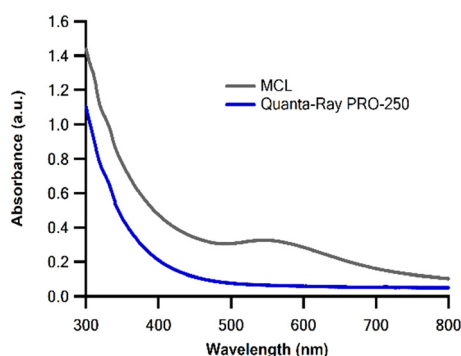
nanostructure was synthesized using 104 mW laser power in a 400 mM polystyrene solution. In order to avoid interference from toluene and ensure uniform polymer concentrations in each sample, the solvent was exchanged for THF and excess polystyrene was removed by filtration after laser ablation. This study employed different excitation wavelengths ranging from 350 nm to 450 nm. It is clearly observed that as the excitation wavelength increased, the emission peaks shifted towards longer wavelengths as shown in Fig. 6(a). The highest fluorescent emission intensity was recorded when the excitation wavelength was set at 330 nm. This indicates that the fluorescence spectra depend on the excitation wavelength, a characteristic commonly reported in the literature on luminescent carbon NPs, similar to carbon dots.[33,34]

Then, the PL spectra of various thicknesses of carbon layers with constant sizes of Au NCs were examined using the previously determined excitation wavelength of 330 nm. In this experiment, all samples were dissolved in THF solvent to eliminate interference from toluene. After laser ablation, excess polystyrene was removed by filtration to ensure the same polymer concentrations were present in each sample. As illustrated in Fig. 6(b), all samples show a primary emission peak around 410 nm and a shoulder peak at approximately 510 nm. Interestingly, as the thickness of the carbon layer decreased, the intensity of the 410 nm emission peak gradually increased, while the intensity of the 510 nm emission peak showed a slower increase. Notably, the peak position remained consistent across samples, as evidenced by the absence of red or blue shifts in the emission peaks with varying carbon layer thicknesses (Fig. 6(b)).[35,36] This may be due to the size difference in all samples not being significant enough to cause a peak shift. In this context, the PL intensity was quantified by measuring a constant
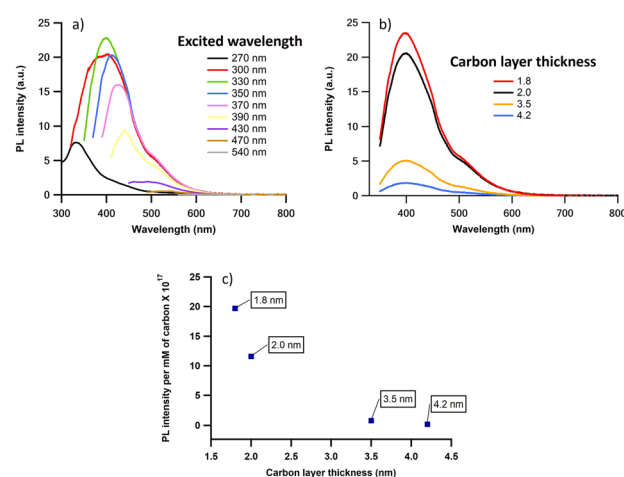

Fig. 5 UV-vis spectrum of carbon-encapsulated Au NCs prepared using the MCL system and Quanta-Ray PRO-250 laser in the presence of polystyrene (400 mM).

Fig. 6 Emission properties of carbon-coated Au NCs obtained by PLAL using MCL in polystyrene/toluene mixture. a) Emission spectra of carbon-coated Au NCs excited at various wavelengths. b) Emission spectra of Au NCs with different carbon layer thicknesses. Excitation wavelength was 330 nm. c) Carbon layer thickness-PL intensity relationship. All the samples were prepared as 0.03 mM Au in THF.

776 | *RSC Appl. Interfaces*, 2025, **2**, 772–779

© 2025 The Author(s). Published by the Royal Society of Chemistry

concentration of Au NCs (0.03 mM). However, since the emission originates from the carbon material, it is crucial to quantify the PL intensity under a fixed carbon content. Experimentally determining the carbon content was difficult, so it was calculated based on the layer thickness for each sample. The emission intensity shown in Fig. 6(b) was then divided by the carbon content in each sample to quantify the PL intensity under fixed carbon content (Fig. 6(c)). As in Fig. 6(b), when the carbon layer thickness is decreased, the 410 nm emission peak intensity gradually increases, following the same pattern as under fixed Au content. Therefore, it is well clear that the PL properties of the carbon-encapsulated Au NCs can be significantly modified by changing the carbon layer thickness. Regarding the fluorescence emission mechanism in carbon quantum dots, bright fluorescence is believed to arise from the radiative recombination of surface-confined electrons and holes.[33,37] In our case, the two fluorescence emissions at approximately 410 and 510 nm likely originate from different excited states. The short-wavelength emission at around 410 nm is hypothesized to originate from nano-sized sp^2 carbon domains, representing intrinsic state emission, while the long-wavelength emission at around 510 nm is attributed to defect state emission due to surface defects.[38]

Conclusions

This study introduces a novel approach for preparing carbon-encapsulated Au NCs *via* PLAL utilizing the MCL system. Controlling NC size and carbon layer thickness is achieved by incorporating polystyrene as a stabilizing agent and toluene as the carbon source. The experimental results reveal that polystyrene concentration strongly influences both the size of Au NCs and the thickness of the carbon layer. Lower laser power combined with higher polystyrene concentration results in smaller Au NCs with thinner carbon layers, demonstrating the effectiveness of this approach. Furthermore, the synthesized nanostructures exhibit enhances photoluminescence properties, showcasing a dependency on excitation wavelength and carbon layer thickness. This study presents a comprehensive investigation into preparing and characterizing carbon-encapsulated metal NCs, highlighting the potential applications and benefits of utilizing MCL-based PLAL techniques. The insights from this investigation into pulse laser ablation in liquids and how laser parameters and solvent properties impact the process will pave the way for the precise synthesis of novel nanostructures.

Experimental

General

Bulk gold rod (99.99% purity), polystyrene (Sigma Aldrich), toluene (Merck Millipore), and tetrahydrofuran (THF) (Merck Millipore) were utilized. All chemicals were used as-is without further purification. Transmission electron

microscopy (TEM) images were captured using a JEOL JEM-2100 electron microscope operated at 200 kV, with samples placed on a holey carbon support film-coated copper microgrid (EMJapan, U1003). Image analysis was performed using ImageJ software, and the mean diameter and standard deviation were calculated from an average of 300 particles. High-resolution TEM images for carbon-encapsulated Au NCs (prepared with 400 mM polystyrene, 104 mW laser power) were acquired using a Hitachi H-9000NAR microscope at 200 kV, again using a holey carbon support film-coated copper microgrid. To enhance contrast, a carbon coating was applied *via* spin-coating with reduced graphene oxide, which minimized the carbon layer's thickness on the copper grid. The carbon coating was performed with following the reported method described in the ref. 39. To investigate the influence of the carbon matrix on the SPR band of the Au NCs, the Mie theory extension for core@shell spheres was applied, considering the carbon as a shell surrounding the Au core (see ESI† for detail).[10] The mean hydrodynamic diameter of the particles in toluene was measured *via* dynamic light scattering (DLS) using a Zetasizer Nano ZS (Malvern, UK) at a wavelength of 633 nm and a detection angle of 173°. Samples were sonicated for 15 min before the measurement. Measurements were averaged over at least three readings at 25 °C. Raman spectra were recorded using a micro-Raman spectrometer (JASCO, NRS-3100) with 532 nm excitation. A drop of the sample solution was dried on a Si wafer surface, and spectra were obtained by averaging 200 scans. For samples containing polystyrene, Raman analysis was performed on Au NCs encapsulated in carbon, prepared using 400 mM polystyrene and 104 mW laser power. The Au NC concentration was determined *via* inductively coupled plasma atomic emission spectroscopy (ICP-AES) using a Shimadzu ICPS-8100. Absorption spectra of the sample solutions were measured using a UV-vis spectrometer (UV-3600, Shimadzu) with a 3.5 mL quartz cuvette. Photoluminescence emission spectra were recorded using a spectrofluorometer (RF-5031PC, Shimadzu) at various excitation wavelengths. For UV-vis and photoluminescence measurements, excess polystyrene was removed by membrane filtration, and the solvent was replaced with THF. Heat capacity measurements were conducted using a differential scanning calorimeter (DSC) (STA 449C Jupiter, Netzsch) under a nitrogen atmosphere. Samples were sealed in aluminium pans, with an empty, hermetically sealed aluminium pan serving as the reference. The measurements were performed over a temperature range of 20 °C to 80 °C at a heating rate of 5 °C min^{-1}. The DSC instrument was calibrated using a sapphire standard prior to the experiments.

General PLAL method

The gold target (5 × 15 mm) underwent cleaning by ultrasonication in acetone for 5 minutes, followed by rinsing

with deionized water and drying before use. Subsequently, the target was affixed onto a custom-made holder (PEEK) equipped with a magnetic stir bar, and this assembly was positioned at the base of a Pyrex® vessel (30 × 80 mm). Zirconia beads (φ 6 mm) were placed between the vessel and the holder to stabilize the rotation axis (Fig. S1(b)†). The liquid level was set to be 5 mm above the gold surface. Laser irradiation was focused directly on the target surface using an Nd:YAG/Cr^{4+}:YAG microchip laser. Additional specifications can be found in the cited papers.[18,19] The initial laser condition to confirm the effect of polystyrene was conducted with the concentration of 50 mM and without polystyrene experiments were conducted under MCL parameters as follows: wavelength of 1064 nm, pulse energy of 1.8 mJ, pulse duration of 900 ps, peak power of >2 MW, and a repetition rate of 100 Hz, with an average power of 180 mW. Laser power effect experiments were carried out with 50 mM of polystyrene at different laser powers (104 mW, 180 mW, 350 mW, and 550 mW) by adjusting the laser current. Polystyrene concentration effect experiments were conducted with concentrations of 10, 50, 100, 200, and 400 mM, utilizing the following laser parameters: wavelength of 1064 nm, pulse energy of 1.0 mJ, pulse duration of 900 ps, peak power of >2 MW, and a repetition rate of 100 Hz, with an average power of 104 mW. Comparative experiments were performed with 400 mM polystyrene using an Nd:YAG laser (Quanta-Ray PRO-250) operating at wavelength, 1064 nm; pulse energy, 1500 mJ; pulse duration, 12 ns; peak power, 125 MW; average laser power, 15 W; repetition rate, 10 Hz. In all experiments, the pulsed laser irradiation onto the gold target was conducted at room temperature for 60 minutes, stirring at 200 rpm.

Data availability

The data supporting this article have been included in the ESI.†

Conflicts of interest

There are no conflicts to declare.

Acknowledgements

Notes and references

1 D. T. Tran, T. Kshetri, N. D. Chuong, J. Gautam, H. V. Hien, L. H. Tuan, N. H. Kim and J. H. Lee, Emerging core-shell nanostructured catalysts of transition metal encapsulated by two-dimensional carbon materials for electrochemical applications, *Nano Today*, 2018, **22**, 100–131.

2 R. Kumar, K. Mondal, P. K. Panda, A. Kaushik, R. Abolhassani, R. Ahuja, H.-G. Rubahn and Y. K. Mishra, Core-shell nanostructures: perspectives towards drug delivery applications, *J. Mater. Chem. B*, 2020, **8**, 8992–9027.

3 T. Zhang, H. Wang, X. Guo, S. Shao, L. Ding, A. Han, L. Wang and J. Liu, Co@C nanorods as both magnetic stirring nanobars and magnetic recyclable nanocatalysts for microcatalytic reactions, *Appl. Catal., B*, 2022, **304**, 120925.

4 G. Li, H. Yang, H. Zhang, Z. Qi, M. Chen, W. Hu, L. Tian, R. Nie and W. Huang, Encapsulation of nonprecious metal into ordered mesoporous n-doped carbon for efficient quinoline transfer hydrogenation with formic acid, *ACS Catal.*, 2018, **8**, 8396–8405.

5 X. Duan, J. Kang, W. Tian, H. Zhang, S. Ho, Y. Zhu, Z. Ao, H. Sun and S. Wang, Interfacial-engineered cobalt@carbon hybrids for synergistically boosted evolution of sulfate radicals toward green oxidation, *Appl. Catal., B*, 2019, **256**, 117795.

6 W. Tian, H. Zhang, Z. Qian, T. Ouyang, H. Sun, J. Qin, M. O. Tadé and S. Wang, Breadmaking synthesis of hierarchically Co@C nanoarchitecture in heteroatom doped porous carbons for oxidative degradation of emerging contaminants, *Appl. Catal., B*, 2018, **225**, 76–83.

7 M. Seipenbusch and A. Binder, Structural stabilization of metal nanoparticles by chemical vapor deposition-applied silica coatings, *J. Phys. Chem. C*, 2009, **113**, 20606–20610.

8 J. F. Li, Y. F. Huang, Y. Ding, Z. L. Yang, S. B. Li, X. S. Zhou, F. R. Fan, W. Zhang, Z. Y. Zhou and D. Y. Wu, Shell-isolated nanoparticle-enhanced Raman spectroscopy, *Nature*, 2010, **464**, 392–395.

9 L. J. Gao and J. H. He, A facile dip-coating approach based on three silica sols to fabrication of broadband antireflective superhydrophobic coatings, *J. Colloid Interface Sci.*, 2013, **400**, 24–30.

10 V. Amendola, G. A. Rizzi, S. Polizzi and M. Meneghetti, Synthesis of gold nanoparticles by laser ablation in toluene: quenching and recovery of the surface plasmon absorption, *J. Phys. Chem. B*, 2005, **109**, 23125–23128.

11 D. Zhang, Z. Li and K. Sugioka, Laser ablation in liquids for nanomaterial synthesis: Diversities of targets and liquids, *JPhys Photonics*, 2021, **3**, 042002.

12 D. Zhang, B. Gökce and S. Barcikowski, Laser synthesis and processing of colloids: Fundamentals and applications, *Chem. Rev.*, 2017, **117**, 3990–4103.

13 X. Xu, L. Gao and G. Duan, The fabrication of au@c core/shell nanoparticles by laser ablation in solutions and their enhancements to a gas sensor, *Micromachines*, 2018, **9**, 278.

14 E. Shiju, N. K. S. Narendran, D. N. Rao and K. Chandrasekharan, Enhanced nonlinear absorption and efficient power limiting action of Au/Ag@ graphite core-shell nanostructure synthesized by laser ablation, *Nano Express*, 2020, **1**, 030026.

15 H. J. Jung and M. Y. Choi, One-pot synthesis of graphitic and nitrogen-doped graphitic layers on nickel nanoparticles produced by pulsed laser ablation in liquid: Solvent as the carbon and nitrogen source, *Appl. Surf. Sci.*, 2018, **457**, 1050–1056.

16 J. F. Li, Y. J. Zhang, S. Y. Ding, R. Panneerselvam and Z. Q. Tian, Core-shell nanoparticle-enhanced raman spectroscopy, *Chem. Rev.*, 2017, **117**, 5002–5069.

17 P. Munnik, P. E. de Jongh and K. P. de Jong, Recent developments in the synthesis of supported catalysts, *Chem. Rev.*, 2015, **115**, 6687–6718.

18 B. S. Hettiarachchi, Y. Takaoka, Y. Uetake, Y. Yakiyama, H. H. Lim, T. Taira, M. Maruyama, Y. Mori, H. Y. Yoshikawa and H. Sakurai, Uncovering gold nanoparticle synthesis using microchip laser system through pulsed laser ablation in aqueous solution, *Ind. Chem. Mater.*, 2024, **2**, 340–347.

19 B. S. Hettiarachchi, Y. Takaoka, Y. Uetake, Y. Yakiyama, H. Y. Yoshikawa, M. Maruyama and H. Sakurai, Mechanistic study in gold nanoparticle synthesis through microchip laser ablation in organic solvents, *Metals*, 2024, **14**, 155.

20 L. H. Sperling, *Introduction to Physical Polymer Science*, Wiley-Inter Science, New York, NY, USA, 1992, p. 87.

21 F. Mafuné, J. Kohno, Y. Takeda, T. Kondow and H. Sawabe, Formation of gold nanoparticles by laser ablation in aqueous solution of surfactant, *J. Phys. Chem. B*, 2001, **105**, 5114–5120.

22 H. Zhang, C. Liang, J. Liu, Z. Tian and G. Shao, The formation of onion-like carbon-encapsulated cobalt carbide core/shell nanoparticles by the laser ablation of metallic cobalt in acetone, *Carbon*, 2013, **55**, 108–115.

23 C.-Y. Shih, R. Streubel, J. Heberle, A. Letzel, M. V. Shugaev, C. Wu, M. Schmidt, B. Gökce, S. Barcikowski and L. V. Zhigilei, Two mechanisms of nanoparticle generation in picosecond laser ablation in liquids: the origin of the bimodal size distribution, *Nanoscale*, 2018, **10**, 6900–6910.

24 C.-Y. Shih, C. Wu, M. V. Shugaev and L. V. Zhigilei, Atomistic modeling of nanoparticle generation in short pulse laser ablation of thin metal films in water, *J. Colloid Interface Sci.*, 2017, **489**, 3–17.

25 B. Bian, J. He, J. Du, W. Xia, J. Zhang, J. P. Liu, W. Li, C. Hu and A. Yan, Growth mechanism and magnetic properties of monodisperse L10-Co(Fe)Pt@C core–shell nanoparticles by one-step solid-phase synthesis, *Nanoscale*, 2015, **7**, 975–980.

26 S. Reichenberger, G. Marzun, M. Muhler and S. Barcikowski, Perspective of Surfactant-Free Colloidal Nanoparticles in Heterogeneous Catalysis, *ChemCatChem*, 2019, **11**, 4489.

27 T. C. Chieu, M. S. Dresselhaus and M. Endo, Raman studies of benzene-derived graphite fibers, *Phys. Rev. B: Condens. Matter Mater. Phys.*, 1982, **26**, 5867–5877.

28 A. Hernando, P. Crespo and M. A. Garcia, Metallic Magnetic Nanoparticles, *Sci. World J.*, 2005, **5**, 972–1001.

29 S. Link and M. A. El-Sayed, Spectral Properties and Relaxation Dynamics of Surface Plasmon Electronic Oscillations in Gold and Silver Nanodots and Nanorods, *J. Phys. Chem. B*, 1999, **103**, 8410–8426.

30 X. Wang, Y. P. Chen and D. D. Nolte, Strong Anomalous Optical Dispersion of Graphene: Complex Refractive Index Measured by Picometrology, *Opt. Express*, 2008, **26**, 22105–22112.

31 H. Tyagi, J. Mohapatra, A. Kushwaha and M. Aslam, Tuning the Observability of Surface Plasmon in Silica-Gold Raspberry Shaped Nanoparticles Using Cuprous Oxide Shell, *ACS Appl. Mater. Interfaces*, 2013, **5**, 12268–12274.

32 K. A. Elsayed, H. Imam, M. A. Ahmed and R. Ramadan, Effect of focusing conditions and laser parameters on the fabrication of gold nanoparticles via laser ablation in liquid, *Opt. Laser Technol.*, 2013, **45**, 495–502.

33 Y.-P. Sun, B. Zhou, Y. Lin, W. Wang, K. A. S. Fernando, P. Pathak, M. J. Meziani, B. A. Harruff, X. Wang, H. F. Wang, P. J. G. Luo, H. Yang, M. E. Kose, B. L. Chen, L. M. Veca and S. Y. Xie, Quantum-Sized Carbon Dots for Bright and Colorful Photoluminescence, *J. Am. Chem. Soc.*, 2006, **128**, 7756.

34 D. Y. Pan, J. C. Zhang, Z. Li, C. Wu, X. M. Yan and M. H. Wu, Observation of pH-, solvent-, spin-, and excitation-dependent blue photoluminescence from carbonnanoparticles, *Chem. Commun.*, 2010, **46**, 3681–3683.

35 L. Bao, Z. L. Zhang, Z. Q. Tian, L. Zhang, C. Liu, Y. Lin, B. Qi and D. W. Pang, Electrochemical tuning of luminescent carbon nanodots: from preparation to luminescence mechanism, *Adv. Mater.*, 2011, **23**, 5801–5806.

36 J. Lu, J. Yang, J. Wang, A. Lim, S. Wang and K. P. Loh, One-Pot Synthesis of Fluorescent Carbon Nanoribbons, Nanoparticles, and Graphene by the Exfoliation of Graphite in Ionic Liquids, *ACS Nano*, 2009, **3**, 2367.

37 L. Cao, X. Wang, M. J. Meziani, F. Lu, H. Wang, P. G. Luo, Y. Lin, B. A. Harruff, L. M. Veca, D. Murray, S.-Y. Xie and Y.-P. Sun, Carbon Dots for Multiphoton Bioimaging, *J. Am. Chem. Soc.*, 2007, **129**, 11318.

38 F. Liu, M. H. Jang, H. D. Ha, J. H. Kim, Y. H. Cho and T. S. Seo, Facile Synthetic Method for Pristine Graphene Quantum Dots and Graphene Oxide Quantum Dots: Origin of Blue and Green Luminescence, *Adv. Mater.*, 2013, **25**, 3657.

39 K. Yamada, M. Okamoto, M. Sakurai, T. Suenobu and K. Nakayama, Solution-processable reduced graphene oxide template layer for molecular orientation control of organic semiconductors, *RSC Adv.*, 2019, **9**, 32940–32945.

© 2025 The Author(s). Published by the Royal Society of Chemistry

RSC Appl. Interfaces, 2025, **2**, 772–779 | 779